Synthesis and Experimental Electron Density of Bis(heterocyclic) Azines: The Case of 6,6′-Bis(chloromethyl)-2,2′-bipyrazine

Florence Bodar-Houillon,[a] Youssef Elissami,[b] Alain Marsura,*[a] Nour Eddine Ghermani,[c] Enrique Espinosa,[c] Nouzha Bouhmaida,[b] and Abdelmalek Thalal[b]

Keywords: 2,2′-Bipyrazine reactivity / Experimental electron density distribution / High-resolution X-ray diffraction / Electron density topology

The synthesis and reactivity of mono- and bis(chloromethyl)-2,2′-bipyrazines toward nucleophiles are reported. The reactivity of the bipyrazine ring is explained in terms of allylic substitution and rearrangement mechanisms. A new family of monofunctionalized bipyrazine derivatives as molecular building blocks for supermolecules has been obtained, opening access to unsymmetrical ligands. The low-temperature crystallographic structure and the experimental electron density distribution of 6,6′-bis(chloromethyl)-2,2′-bipyrazine have been determined on the basis of high-resolution X-ray diffraction data. The electron density of the molecule has been accurately analyzed using the topological properties of its gradient and Laplacian features. The reactivity of these bidentate molecules in metal complexation is related to the shape of the atomic basins and may be explained in terms of a key/lock-type interaction. The results are compared with corresponding data for 2,2′-dimethyl-6,6′-diphenyl-4,4′-bipyrimidine.

The synthesis and chemistry of bis(heterocycles) is of considerable interest with regard to the construction of new supramolecular structures, as well as of strongly fluorescent lanthanide cryptates or podates,[1a−1d] and of self-assembling metal complexes[2a,2b] in the form of helices,[3a−3d] grids,[4] ladders,[5] etc. Among the bis(heterocycle) ligands, 2,2′-bipyrazine is less well studied and less often employed compared to other bis(monoazines) (e.g. bipyridine, phenanthroline, etc.). However, the recent incorporation of 2,2′- and 4,4′-bipyrimidine and 2,2′-bipyrazine moieties[6,7a−7d,8] into the backbones of supramolecular architectures has given rise to interesting additional properties. For example, enhanced fluorescence photophysical properties have been observed in new lanthanide complexes,[9] new complexation properties have recently been reported for metal-chelating, self-assembling supramolecular structures,[10] and a new class of receptors has been developed.[11] In continuation of our research into bidendate ligands as new building blocks for constructing supramolecular assemblies, the present paper deals with the chemical reactivity of 6,6′-bis(chloromethyl)- (**2**) and 6-chloromethyl-2,2′-bipyrazine (**3**) derivatives towards nucleophiles. Moreover, the mechanisms of these reactions are assessed on the basis of the results of chemical and high-resolution crystallographic studies.

Considering aspects of the synthesis of bipyrazine molecular building blocks, we set out (i) to follow a strategy based on sequential Williamson condensations between bipyrazine monoalcoholate or dialcoholate (vs. monothiolate, dithiolate) components and monochloride or dichloride components in order to obtain oligobipyrazine ligands such as the trimeric ligand **22** (see below), and (ii) to synthesize the diamino-2,2′-bipyrazine unit with the aim of constructing new unsymmetrical cryptands using the one-step condensation (1 equiv. diamine + 2 equiv. dichloride). Surprisingly, the reactivity of **3** in the presence of various nucleophiles led to the generation of positional isomers of the bis(heterocycle), thereby potentially opening a route to chemically active monofunctionalized bipyrazine ligands. Thus, we decided to explore this avenue of investigation, mainly in view of its great potential with regard to anchoring reactions of cryptands that might allow us to introduce unambiguous, stoichiometric binding sites on specific supports or soluble biomolecules. Furthermore, low-temperature high-resolution X-ray data have been used to derive the electron density of **2** in the solid state. The topological electron density characteristics have been scrutinized in order to understand further the particular reactivity of bipyrazine. No reports have hitherto described the synthesis and reactivity of such units and we hope that this work will be helpful with regard to the design of new series of ligands.

[a] Unité Mixte de Recherche CNRS-7565, Structure et Réactivité des Systèmes Moléculaires Complexes, Université Henri Poincaré, Nancy 1,
5, Rue Albert Lebrun, B. P. 403, F-54001 Nancy, France
Fax: (internat.) + 33-3/83178863
E-mail: marsura@srsmc.u-nancy.fr
[b] Laboratoire des Sciences des Matériaux, Université Cadi Ayyad, Faculté des Sciences Semlalia,
Boulevard Prince Moulay Abdallah, B. P. S15, 40000 Marrakech, Morocco
E-mail: ucadp@cybernet.net.ma
[c] Laboratoire de Cristallographie et Modélisation des Matériaux Minéraux et Biologiques, LCM^{3}B, UPRES A CNRS 7036, Université Henri Poincaré, Nancy 1, Faculté des Sciences,
Boulevard des Aiguillettes, B. P. 239, F-54506 Vandoeuvre-lès-Nancy Cedex, France
Fax: (internat.) + 33-3/83178817
E-mail: ghermani@lcm3b.u-nancy.fr

Supporting information for this article is available on the WWW under http://www.wiley-vch.de/home/eurjoc or from the author.

  1434−193X/99/0606−1427 $ 17.50+.50/0

Results and Discussion

Synthesis

The starting chloromethyl derivatives **2** and **3** were obtained from 6,6′-dimethyl-2,2′-bipyrazine (**1**) by a radical chlorination reaction.[8] All the synthesized products (Scheme 1), apart from the thio (**20**, **21**) and amino compounds (**17**, **19**) and the trimeric ligand **22**, were obtained from **2** or **3** in good to moderate yields by direct nucleophilic displacement reactions under various conditions. (see Experimental Section). In all cases, the reaction yields a mixture of isomeric substituted compounds as a result of two mechanisms, namely a first-order nucleophilic substitution (S_N1) at the allylic carbon atom, and a first-order allylic rearrangement (S_N1') in which the nucleophile attacks at a γ- or ε-carbon atom[12] (Scheme 2). The experimental conditions clearly indicate that the reaction occurs under S_N1 conditions (thermodynamic control) and furnishes, as predicted in this case, isomeric mixtures arising from attack of the nucleophile on stabilized intermediate allylic carbocations (Scheme 2). Furthermore, the relative amounts of the isomers obtained (Table 1), irrespective of the solvent used, are in good agreement with the expected relative stabilities of the allylic carbocation intermediates ($C1^+ > C3^+ > C2^+$) and conform to the so-called "product spread" phenomenon.[13] Finally, it should be pointed out that the resulting monosubstituted 6,6′-dimethyl derivatives may be halogenated for a second time, leading to 6,6′-bis-(halogenomethyl) units, which represent desirable building blocks for the regiospecific construction of monofunctionalized supramolecular species.

In other systems, it is well known that a nucleophilic substitution at an allylic carbon atom can also take place according to an S_N2 mechanism, without any allylic rearrangement. This seems to be the case in the present nucleophilic substitution leading exclusively to the 6,6′-diazido isomer **18** in high yield, as well as that giving the trimeric compound **22**. The latter is obtained by the reaction of bipyrazine alcoholates with 6,6′-bis(iodomethyl)-2,2′-bipyrazine in dipolar aprotic solvents. Furthermore, allylic re-

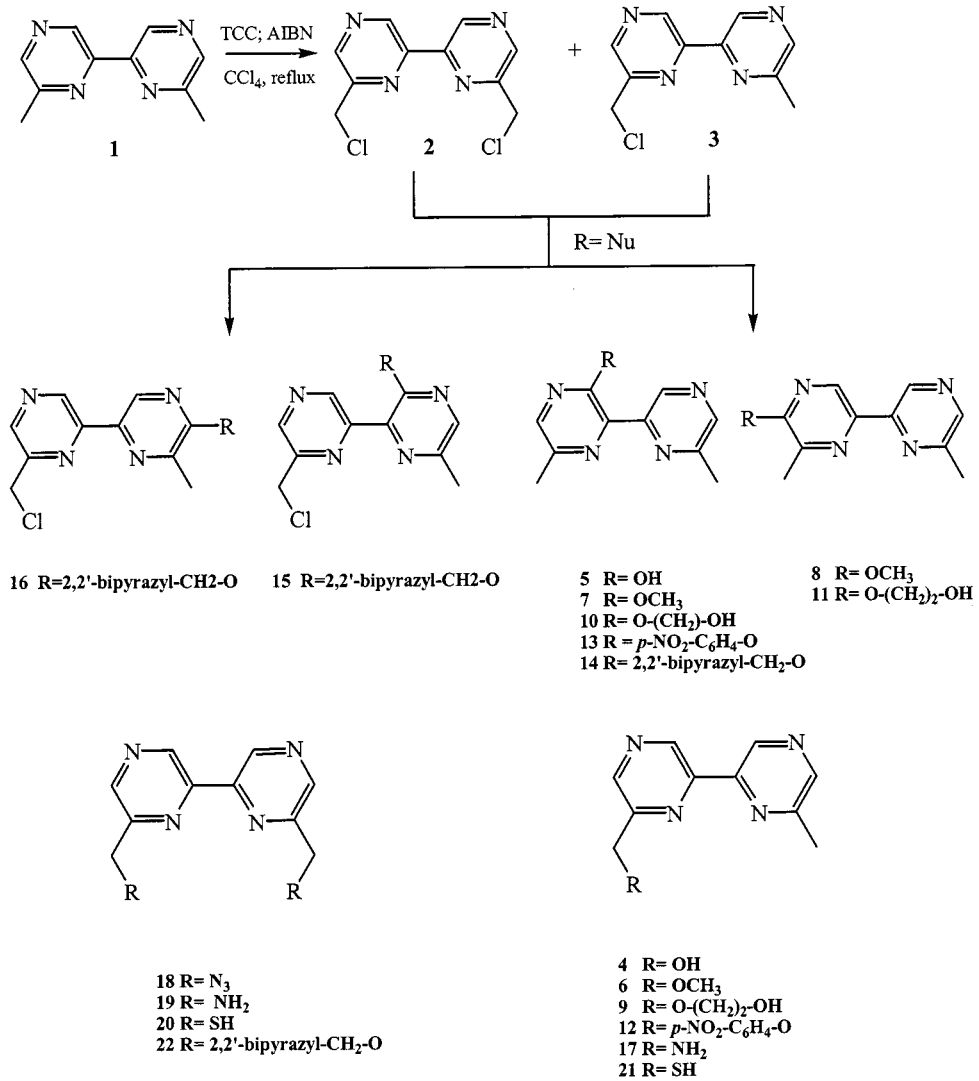

Scheme 1. Synthesized products

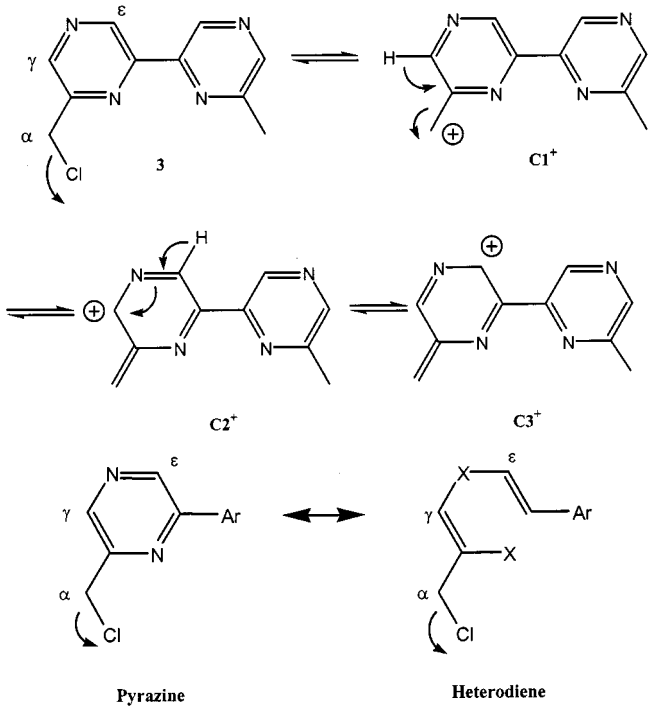

Scheme 2. Reactivity mechanisms

Table 1. Ratios of 2,2′-bipyrazine isomers obtained by nucleophilic displacement reactions of 2,2′-bipyrazine dihalide **2** and monohalide **3**

Nucleophile	Solvent	R^1, R^2	Relative isomer ratio in%[a] (6)	(5)	(3)
OH^-	CH_3CN/H_2O	Cl, H	47	0	18
CH_3O^-	anhyd. CH_3OH	Cl, H	59	20	21
$HO(CH_2)_2O^-$	$HO(CH_2)_2OH$	Cl, H	41	17	18
p-$NO_2(C_6H_4)O^-$	anhyd. CH_3CN	Cl, H	35	0	12.5
N_3^-	CH_3SOCH_3	Cl, Cl	77	0	0
Bipyrazyl-CH_2O^-	anhyd. THF	Cl, H	0	ca. 1	10
Bipyrazyl-CH_2O^-	anhyd. THF	Cl; Cl	0	31	21

[a] (6), (5), and (3) are positions of substitution on the bipyrazine ring.

arrangement could also take place under S_N2 conditions by attack at the γ- or ε-carbon atom rather than at the usual α position. This mechanism is called second-order allylic rearrangement (S_N2').[14] It is sometimes encountered when there is a sterically hindered α substituent present, when a large nucleophile is used, or when certain leaving groups are attached at the allylic carbon atom.[13] In the present case, the second situation appears to be operative; the bulky bipyrazine alcoholate nucleophile anion gives specifically the isomers **14** to **16**, which arise from an allylic rearrangement process. One or two of the above factors are probably responsible for determining the second-order-type mechanisms that take place preferentially in these cases.

Another interesting point that merits discussion is that the reactivity of the bipyrazine system differs greatly from that of a true aromatic system. Indeed, bipyrazines react preferentially as unconjugated heterodienes (Scheme 2b). From a chemical point of view and for the sake of comparison, it is noteworthy that the previously studied 2,2′-dimethyl-4,4′-bipyrimidine[7a] only undergoes substitution at its 2,2′-methyl positions. No substitution takes place at the other free carbon positions on the heterocycle ring. These results and the lack of described reactions of this type with other bis(heterocycles) (e.g. bipyridine, phenanthroline, etc.) reflect the unique reactivity of the bipyrazine system.

Molecular Conformation and Crystal Stacking

Figure 1 shows an ORTEP[15] representation and the labelling scheme of the 6,6′-bis(chloromethyl)-2,2′-bipyra-

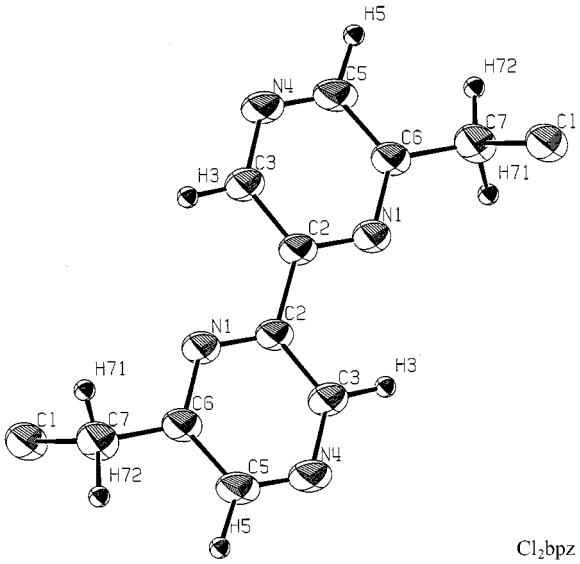

Figure 1. ORTEP view of 6,6′-bis(chloromethyl)-2,2′-bipyrazine

Table 2. Principal bond lengths [Å] and angles [°] in 6,6′-bis(chloromethyl)-2,2′-bipyrazine; the estimated standard deviations are given in parentheses

	distance		distance
N1−C2	1.3349(5)	N4−C3	1.3332(6)
N1−C6	1.3372(5)	N4−C5	1.3369(6)
C2−C3	1.4008(5)	C5−C6	1.3964(5)
C6−C7	1.4949(5)	C7−Cl	1.8080(5)
C2−C2′[a]	1.4765(7)		

	angle
C6−N1−C2	117.14(3)
N1−C2−C3	121.32(3)
N1−C2−C2′[a]	117.74(4)
C3−C2−C2′[a]	120.94(4)
C2−C3−N4	121.64(4)
C3−N4−C5	116.68(4)
N4−C5−C6	121.88(4)
C5−C6−N1	121.14(3)
C7−C6−N1	117.42(3)
C7−C6−C5	121.44(4)
C6−C7−Cl	109.07(3)

[a] Symmetry operation between the two pyrazine rings: $-x$, $2-y$, $-z$.

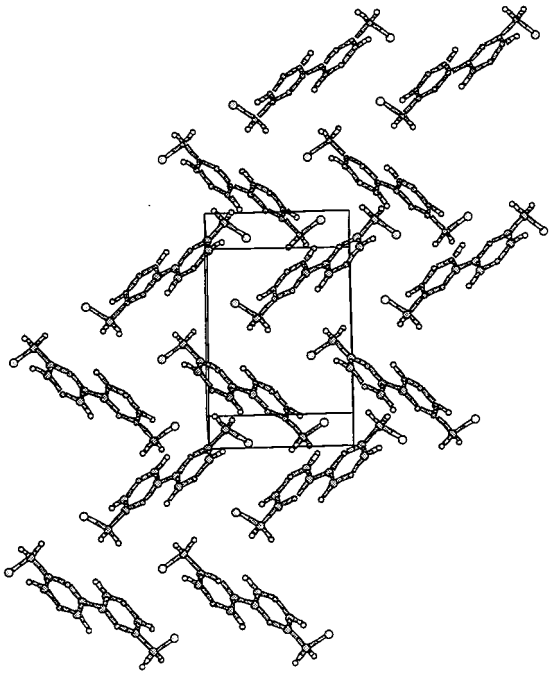

Figure 2. Molecular stacking in the crystal of 6,6′-bis(chloromethyl)-2,2-bipyrazine

zine (Cl_2bpz) molecule. The molecule adopts an *s-trans* conformation in the crystalline state. The two connected pyrazine rings, related by the symmetry operation ($-x$, $2 - y$, $-z$), are planar, with a crystallographic center of inversion being situated in the middle of the $C^2-C^{2\prime}$ vector. C^7 and $C^{7\prime}$ lie in the plane of the pyrazine rings, but the chlorine atoms reside 1.75 and −1.75 Å from the mean plane of the molecule defined by $N^1-C^2-C^{2\prime}$. Table 2 gives the main bond lengths and angles obtained after multipolar refinement (see Experimental Section). C−N and C−C bond lengths in the pyrazine ring are in good agreement with those reported for 2,2′-dimethyl-6,6′-diphenyl-4,4′-bipyrimidine (Ph_2bpm),[16] but the C−C bond lengths are slightly longer than those reported in a study of pyrazines by De With et al.[17] We note, however, that the $C^2-C^{2\prime}$ distance of 1.4765(7) Å is shorter than the distance found between the corresponding carbon atoms in Ph_2bpm [1.4891(7) Å].[16] The C^7-Cl distance of 1.8080(5) Å is significantly shorter than the C−Cl distance of 1.8421(7) Å found in dichlorodioxane,[18] the bond length in which is increased owing to the anomeric effect. In the solid state, stacking gives rise to two almost perpendicular planes, in which the molecules are arranged as shown in Figure 2 (here, only the cell translations $\pm b$ and $\pm c$ are considered for the sake of clarity). Each plane corresponds to one of the two molecules in the unit cell. In the intermolecular region, the chlorine atom is surrounded by three hydrogen atoms: $Cl-H^3$ ($-0.5 - x$, $1.5 + y$, $0.5 - z$) = 2.7551(1) Å; $Cl-H^{71}$ ($0.5 - x$, $-0.5 + y$, $0.5 - z$) = 2.8846(1) Å; $Cl-H^5$ ($-1 + x$, y, z) = 2.9251(1) Å. The two chlorine atoms of a given Cl_2bpz molecule are directed towards the centers of the pyrazine rings of the two neighbouring parallel molecules (Figure 2).

Experimental Electron Deformation Density

Table 3 lists the multipolar parameters for Cl_2bpz, which were used to calculate the static electron deformation density by means of the STATDENS program.[19] Following the multipolar refinement, the atomic thermal motion and the electron density distribution are deconvoluted. Thus, the static bond deformation electron densities are generally comparable to those derived from high-level ab initio SCF theoretical calculations.[20] Figure 3 shows the static electron deformation density in the plane of the pyrazine ring of Cl_2bpz after the multipolar refinement. The main features of this map are the good resolution of the nitrogen lone pairs and a more pronounced concentration of electrons in the C^5-C^6 and C^2-C^3 bonds of the pyrazine ring. The electron peak heights reach 1.2 $eÅ^{-3}$ in the C^5-C^6 and C^2-C^3 bonds [C^5-C^6 = 1.3964(5) Å, C^2-C^3 = 1.4008(5) Å]. The longest C−C bonds in the Cl_2bpz molecule exhibit

Table 3. P_{lm} and κ multipolar parameters for 6,6′-bis(chloromethyl)-2,2′-bipyrazine after multipole refinement

	N4	N1	C7	C6	C5	C3	C2	Cl	H71	H72	H5	H3
κ	0.986(5)	0.988(5)	0.97(1)	1.01(1)	0.99(1)	0.99(1)	0.99(1)	0.985(5)	1.29(9)	1.31(9)	1.41(9)	1.12(5)
κ′	1.07(5)	0.95(4)	0.99(5)	0.96(5)	0.87(3)	0.99(5)	1.02(5)	1.14(5)	1.000	1.000	1.000	1.000
P_{val}	5.06(7)	5.08(7)	4.46(18)	3.68(14)	4.35(14)	3.93(13)	4.13(9)	7.33(6)	0.61(9)	0.80(10)	0.64(9)	0.93(9)
dX	−0.09(1)	−0.19(2)	0.00(3)	0.02(2)	−0.04(4)	0.03(2)	0.06(2)	0.02(2)	0.01(3)	0.15(4)	0.07(3)	0.20(3)
dY	−0.05(2)	−0.03(2)	−0.13(2)	0.03(3)	0.12(3)	−0.03(3)	0.06(3)	−0.03(2)	0.00(2)	−0.20(3)	−0.02(2)	0.05(3)
dZ			0.02(3)					−0.02(2)	0.10(2)	−0.07(2)	−0.11(2)	0.03(2)
Qz_2	−0.16(1)	−0.17(2)	0.13(2)	−0.27(3)	−0.32(3)	−0.20(3)	−0.14(2)	0.10(2)				
QZX			0.05(3)					0.02(2)				
QZY			−0.03(2)					−0.03(2)				
QXX−YY	0.05(1)	0.05(1)	0.07(2)	−0.02(2)	0.07(3)	0.02(3)	0.00(2)	−0.08(2)				
QXY	−0.03(1)	−0.01(1)	−0.07(2)	−0.02(2)	0.03(2)	−0.02(2)	0.05(3)	0.07(2)				
OZZZ			0.05(2)					−0.02(2)				
OXZZ	−0.04(1)	−0.05(1)	−0.19(3)	0.00(2)	−0.06(2)	−0.01(2)	0.00(2)	−0.08(2)				
OYZZ	−0.02(1)	−0.02(1)	−0.19(3)	−0.04(2)	0.08(2)	0.04(2)	0.03(2)	0.04(1)				
OZ(XX−YY)			0.02(2)					−0.02(1)				
OXYZ			0.05(2)					0.01(1)				
OXXX	−0.11(1)	−0.10(1)	0.19(3)	−0.38(2)	−0.49(5)	−0.30(4)	−0.31(4)	0.10(2)				
OYYY	−0.01(1)	−0.05(1)	0.08(2)	−0.06(2)	−0.03(3)	−0.04(2)	−0.04(2)	−0.00(1)				

electron density peak heights of 0.7 eÅ^{-3}, i.e. in $C^2-C^{2'}$ [$C^2-C^{2'}$ = 1.4765(7) Å] and C^6-C^7 [C^6-C^7 = 1.4949(5) Å]. These values are in good agreement with those generally observed for C−C single bonds in peptide molecules.[21] On the other hand, the electron density peak heights in the C−N bonds fall in the range 0.7−0.9 eÅ^{-3} and their maxima are situated 0.5 Å from the carbon nuclei. We note that the electron deformation density in the C−N bonds of the pyrazine rings is systematically polarized towards the carbon atoms (Figure 3). Differences in electron density peak heights between the C−C and C−N bonds in the pyrimidine ring of Ph_2bpm[16] were not observed (on average 0.65 eÅ^{-3} in both the C−C and C−N bonds). Even though the bond lengths in pyrazine and pyrimidine rings are quite similar, the electron deformation density distribution seems to be different with respect to the locations of the nitrogen atoms. Compared to the pyrimidine ring in Ph_2bpm, the pyrazine ring in Cl_2bpz displays less aromatic character. The C^2-C^3 and C^5-C^6 aromatic bonds and the clockwise polarization of the electron density in the $N^1-C^6-C^5$ and $N^4-C^3-C^2$ arms are in good agreement with the expected chemical reactivity of Cl_2bpz at its γ (C^5) and ε (C^3) positions, which constitute an unconjugated heterodienic-like system (Scheme 2). Moreover, these two sites are significantly differentiated by the valence populations (P_{val} in Table 3), corresponding to net charges of −0.35(14) and +0.07(13) e for the γ and ε sites, respectively. In contrast to our results, the experimental electron deformation density derived for pyrazine on the basis of X-ray diffraction data obtained at 184 K by Moss et al.[22] did not show a distinction between C−C and C−N bonds. This discrepancy is probably due to the high degree of atomic thermal motion in the pyrazine molecule at this temperature.

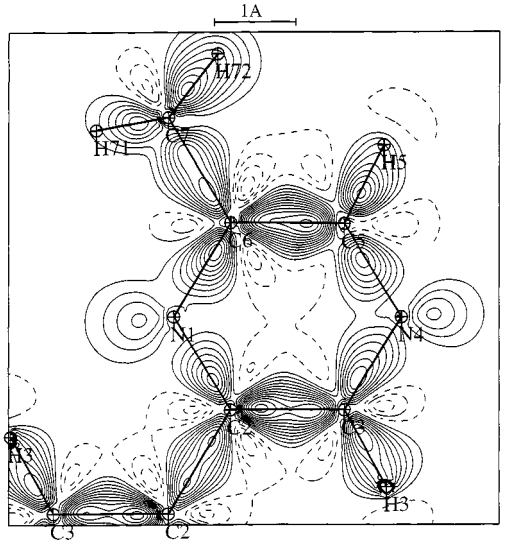

Figure 3. Static electron deformation density in the pyrazine ring of the 6,6′-bis(chloromethyl)-2,2-bipyrazine molecule; contour intervals ±0.1 eÅ^{-3}; negative contours are dashed, zero contour omitted

Topological Analysis of the Electron Density

In the framework of quantum theory, topological analysis of the electron density ρ(**r**), as developed by Bader,[23] permits characterization of individual atoms in molecules and crystals. Interatomic interactions may be studied through the topological properties of ρ(**r**) at the bond critical points $\mathbf{r}_{CP}$, i.e. the points of zero-gradient $\nabla\rho(\mathbf{r}_{CP}) = 0$.

After multipolar modelling of the experimental electron density derived from X-ray diffraction data, we analyzed this fundamental property in the Cl_2bpz molecule using the PROP program,[24] which calculates the gradient $\nabla\rho(\mathbf{r})$ and the Laplacian $\nabla^2\rho(\mathbf{r})$ of the electron density. We focused on the shape of the basin of the nitrogen atoms in the molecule with a view to predicting the metal complexation reactivity. For comparison purposes, the topological properties of the pyrimidine ring in Ph_2bpm are also reported.

The electron deformation density distribution in a molecule depends only on the atomic valence orbitals and the charge transfer amongst the atoms. However, the quantum mechanical properties of a system are based on its total electron density and hence characterization of the atomic and molecular bonds should be based on this latter observable quantity. Consequently, we analysed the interatomic interactions in the Cl_2bpz molecule, as well as the reactivity of the nitrogen atoms of the pyrazine ring, in terms of the topological properties of the total electron density ρ(**r**) at their (3,−1)-CPs [$\rho(\mathbf{r}_{CP})$, the Laplacian $\nabla^2\rho(\mathbf{r}_{CP})$, and the eigenvalues of the Hessian matrix, $\lambda_1(\mathbf{r}_{CP})$, $\lambda_2(\mathbf{r}_{CP})$, $\lambda_3(\mathbf{r}_{CP})$] and the gradient vector field $\nabla\rho(\mathbf{r})$. Table 4 gives the topological properties of the electron density at the (3,−1)-CPs in the rings of both Cl_2bpz and Ph_2bpm, as well as the distances of the nuclei from these critical points. As the CP is situated on the interatomic surface, the longer the distance to the nucleus, the more extended the basin is in that direction. Whereas among the C−N bonds the total electron density is systematically more concentrated in the pyrimidine ring of Ph_2bpm than in the Cl_2bpz pyrazine ring [$\nabla^2\rho(\mathbf{r}_{CP})$ values are more negative and $\rho(\mathbf{r}_{CP})$ values are higher in the former compound], the C^2-C^3 and C^5-C^6 bonds in Cl_2bpz show a concentration of charge similar to that found in the C^4-C^5 and C^5-C^6 bonds of Ph_2bpm. We note, however, that a localization of the double-bond character in the rings is not apparent from these values. On the other hand, the single C−C bond Laplacian $\nabla^2\rho(\mathbf{r}_{CP})$ and the electron density values $\rho(\mathbf{r}_{CP})$ at the critical points of the $C^2-C^{2'}$ bond in Cl_2bpz [$\nabla^2\rho(\mathbf{r}_{CP}) = -14.4$ eÅ^{-5}, $\rho(\mathbf{r}_{CP}) = 1.80$ eÅ^{-3}] reveal similar concentration of electron density than that found in the corresponding $C^4-C^{4'}$ bond [$\nabla^2\rho(\mathbf{r}_{CP}) = -15.7$ eÅ^{-5}, $\rho(\mathbf{r}_{CP}) = 1.92$ eÅ^{-3}] linking the pyrimidine rings in Ph_2bpm. The same holds true for C−C linkages when only one carbon atom belongs to the ring: C^6-C^7 [$\nabla^2\rho(\mathbf{r}_{CP}) = -14.5$ eÅ^{-5}, $\rho(\mathbf{r}_{CP}) = 1.79$ eÅ^{-3}] in Cl_2bpz and C^2-C^{13} [$\nabla^2\rho(\mathbf{r}_{CP}) = -16.4$ eÅ^{-5}, $\rho(\mathbf{r}_{CP}) = 1.93$ eÅ^{-3}] in Ph_2bpm. Topological properties at the C−H bond CPs involving a carbon atom of pyrimidine or pyrazine ring have similar values of $\nabla^2\rho(\mathbf{r}_{CP}) = -19.0$ eÅ^{-5}, $\rho(\mathbf{r}_{CP}) = 1.9$ eÅ^{-3} for C^5-H^5 in Ph_2bpm and C^3-H^3 in Cl_2bpz, respec-

Table 4. Topological properties in Cl_2bpz and Ph_2bpm: distances from the critical point to the nuclei, the eigenvalues 1, 2, 3, the values of the Laplacian $\nabla^2\rho(\mathbf{r}_{CP})$, and the electron density $\rho(\mathbf{r}_{CP})$ at the bond critical point CP

(3,−1) CP	A-B	d_A [Å]	d_B [Å]	λ_1 [eÅ^{-5}]	λ_2 [eÅ^{-5}]	λ_3 [eÅ^{-5}]	$\nabla^2\rho$ [eÅ^{-5}]	$\rho(\mathbf{r}_{CP})$ [eÅ^{-3}]
Cl_2bpz	N4−C5	0.777	0.561	−18.0	−17.6	14.3	−21.3	2.26
	N4−C3	0.787	0.548	−18.9	−15.9	16.0	−18.9	2.25
	N1−C6	0.759	0.578	−19.0	−17.6	15.3	−21.4	2.30
	N1−C2	0.761	0.574	−17.8	−15.9	14.7	−19.0	2.19
	C6−C7	0.756	0.740	−12.8	−11.8	10.0	−14.5	1.79
	C6−C5	0.679	0.717	−18.5	−14.1	9.8	−22.9	2.23
	C5−H5	0.707	0.370	−18.4	−16.1	19.9	−14.5	1.83
	C3−C2	0.685	0.716	−17.7	−14.1	11.0	−20.8	2.18
	C3−H3	0.702	0.375	−17.8	−16.1	14.5	−19.4	1.85
	C2−C2	0.738	0.738	−14.3	−10.9	10.9	−14.4	1.80
Ph_2bpm	N1−C2	0.724	0.615	−23.4	−19.3	20.3	−22.4	2.52
	N1−C6	0.730	0.615	−22.7	−19.2	19.9	−22.0	2.49
	N3−C2	0.747	0.592	−25.1	−20.3	19.9	−25.5	2.56
	N3−C4	0.757	0.587	−23.3	−19.8	19.2	−23.9	2.50
	C2−C13	0.774	0.721	−15.9	−14.2	13.7	−16.4	1.93
	C4−C4′	0.745	0.745	−16.2	−13.6	14.1	−15.7	1.92
	C4−C5	0.712	0.681	−20.1	−15.1	13.5	−21.7	2.27
	C5−C6	0.692	0.709	−20.4	−16.1	13.8	−22.7	2.29
	C5−H5	0.741	0.335	−20.1	−18.7	19.8	−19.0	1.91
	C6−C7	0.785	0.696	−16.1	−13.3	14.2	−15.0	1.91

tively, but the Laplacian value is different for C^5-H^5 in Cl_2bpz [$\nabla^2\rho(\mathbf{r}_{CP}) = -14.5$ eÅ^{-5}].

Figure 4 shows the gradient vector field of the electron density $\nabla\rho(\mathbf{r})$ calculated for solid-state *s-trans* conformation Cl_2bpz (Figure 4a) and Ph_2bpm (Figure 4b), respectively. In the Cl_2bpz molecule (Figure 4a), whereas the atomic basin associated with the inner nitrogen atom N^1 presents a less extended surface towards the intermolecular region, than the corresponding N^4 basin surface. On the other hand, the atomic volumes associated with both the outer N^1 and inner N^3 nitrogen atoms in the Ph_2bpm molecule (Figure 4b) have a closed shape, comparable to the basin of N^1 in Cl_2bpz. We note, however, that the atomic volume of the outer nitrogen N^1 in Ph_2bpm is expected to be of closed form because of the proximity of the surrounding methyl group and the phenyl ring. This is not the case for the outer nitrogen atom N^4 in the Cl_2bpz molecule. Given the property of the gradient function, the open or closed characters of these atomic volumes can be directly related to the concavity or convexity of the atomic electron density towards the intermolecular space.

The previous electron density study of Ph_2bpm[16] allowed predictions to be made concerning the complexation of a copper cation by such a molecule. We based our arguments on the electrostatic potential features calculated for the molecule in the *s-cis* conformation, although the modelling of the electron density was performed on the solid-state *s-trans* conformation. The interaction properties of the pyrimidine ring in the Ph_2bpm molecule are seemingly unaffected by the artificial rotation by 180° of one ring with respect to the other. A previous study of Ph_2bpm led to a low value for the rotational energy barrier[25] about the $C^4-C^{4\prime}$ axis connecting the two pyrimidine rings in this molecule. Both the inner and outer nitrogen atoms participate in metal complexation, as was demonstrated in a structural study of the copper(I)/2,2′-dimethyl-4,4′-bipyrimidine complex.[7d] From an electrostatic point of view, the net

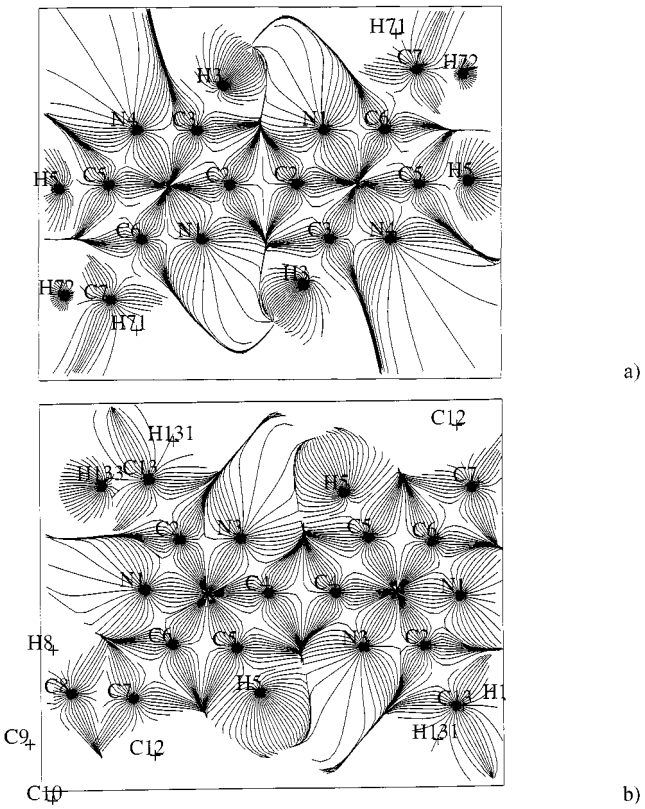

Figure 4. Gradient field of the total electron density in: a) 6,6′-bis(chloromethyl)-2,2-bipyrazine and b) 2,2′-dimethyl-6,6′-diphenyl-4,4′-bipyrimidine; solid-state *s-trans* conformation

charges for the nitrogen atoms in the Ph_2bpm molecule were determined as −0.31(2) e for N^3 and −0.21(2) e for N^1, respectively, as opposed to the almost neutral N^1 and N^4 nitrogen atoms in Cl_2bpz found in the present study (Table 3). With a view to understanding the complexation behaviour of the Ph_2bpm and Cl_2bpz molecules, we have calculated the gradient of the electron density in the *s-cis*

conformation, assuming that the electron density in the rings is not sensitive and, to a first approximation, is not modified by the rotation of one ring with respect to the other. The analysis will be based on the gradient of the electron density. A previous study by Aray and Bader,[26] analysed the adsorption of CO molecules onto MgO surfaces using also the gradient of the electron density. They reported that a Lewis acid/base reaction corresponds to a build-up of charge on the base and a charge depletion on the acid. They found that the exposed charge concentration on the carbon atom interacts with the region of charge depletion or *hole* in the outer shell of the charge concentration on the Mg atom, creating a closed-shell interaction. The gradient vector field maps of $\rho(\mathbf{r})$ for the MgO (100) surface before and after the CO adsorption unambiguously illustrate how the interaction takes place at Mg, in that the atom has a symmetrically convergent interatomic surface extending into the intermolecular region. Figure 5 shows the $\nabla\rho(\mathbf{r})$ field calculated in the plane of the rings for Cl_2bpz (Figure 5a) and Ph_2bpm (Figure 5b) molecules in *s-cis* conformation. Here, we observe a symmetrical convergent interatomic surface extending into the intermolecular region for N^3,$N^{3'}$ and N^1 of Ph_2bpm and for N^1,$N^{1'}$ of Cl_2bpz, but a divergent interatomic surface for N^4 of Cl_2bpz. In our previous work,[7] we reported inner and outer nitrogen Cu−N distances ranging from 2.04 to 2.08 Å. If we place a hypothetical copper cation at a distance of 2 Å from N^1 and N^4, as in Figure 5a (Cl_2bpz), or at 2 Å from N^1 and N^3, as in Figure 5b (Ph_2bpm), it will lie within the atomic basins of the nitrogen atoms in all cases. However, the main difference appears when we look at the gradient vector field topologies at this distance: The reactive nitrogen atoms in Ph_2bpm present a concave $\rho(\mathbf{r})$ surface towards the intermolecular region, which adapts well to the convex $\rho(\mathbf{r})$ surface of a non-chemically bonded cation (as a key/lock system). In the Cl_2bpz molecule, it can clearly be seen that the couple N^1,$N^{1'}$ satisfies this rule, but that N^4 can be expected to be non-reactive (Figure 5a) because of a convex electron density at this distance. Furthermore, the low electron density that we found in the intermolecular region at a distance of 2 Å from the nitrogen nuclei (less than 0.05 $e\text{Å}^{-3}$) is also favourable with regard to an interaction with a hypothetical metal cation at this distance without major changes in the $\rho(\mathbf{r})$ distribution, i.e. with minimal energy cost. Without any electrostatic considerations, a substituent such as a methyl group near the outer nitrogen atom of 2,2′-pyrazine would probably enhance the concavity (key/lock system) of the electron density around this atom and thereby improve its reactivity, as was found for the external nitrogen atom N^1 in Ph_2bpm.

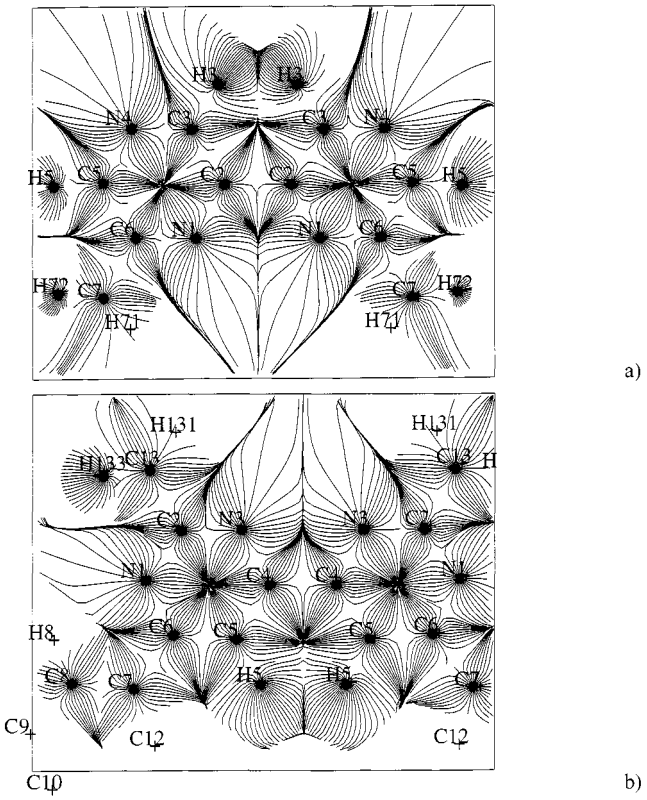

Figure 5. Gradient field of the total electron density in: a) 6,6′-bis(chloromethyl)-2,2-bipyrazine and b) 2,2′-dimethyl-6,6′-diphenyl-4,4′-bipyrimidine; solid-state *s-cis* conformation

Conclusion

The investigated chloromethyl bipyrazine derivatives represent useful molecules for obtaining monofunctionalized bidendate bipyrazine units. They are more easily accessible than our previously studied systems leading to monofunctionalized bipyridines.[27] Regarding the reactivity of the 2,2′-bipyrazine unit towards nucleophiles, both the chemical behavior and the experimental electron density clearly point to greater non-aromatic character of this heterocycle compared to other diazines such as pyrimidines, and probably also monoazines such as bipyridine and phenanthroline. Topological analysis of the electron density has allowed a qualitative description and a comparison of the coordination power of the inner and outer nitrogen atoms of the bipyrazine and the previously studied 4,4′-bipyrimidine rings. This description has highlighted the influence of substituent proximity on the electron density concavity at the nitrogen sites. This topological description should be useful in predicting the metal complexation capacity of a given nitrogen atom in a diazine, and should prove advantageous with regard to heterotopic bidendate mixed ligands such as bpz−byp or bpz−bpm or bpz. The latter, as well as their metal complexes, are currently under investigation.

Experimental Section

General Aspects: All solvents were distilled prior to use; anhydrous solvents were distilled under argon and then stored over molecular sieves (3−4 Å). − Column chromatography (CC): Merck silica gel 60 (0.040−0.063 mm). − Analytical thin-layer chromatography (TLC): Merck silica gel or alumina 90 plates; detection by UV light (254 nm). − Melting points: Kofler hot-stage apparatus. − ^{1}H-NMR spectra: Bruker DRX400 and AM250 instruments; chemical shifts in parts per million relative to residual proton signal of sol-

vent as internal reference (^{1}H: $CHCl_3$ in $CDCl_3$, δ = 7.26); coupling constants *J* in Hertz. − Mass spectrometry: EI-MS was performed by the Service Commun de l'Université Henri Poincaré, Nancy 1. − Microanalyses were performed by the Service Central de Microanalyses du CNRS, Vernaison. − 6,6′-Dimethyl-2,2′-bipyrazine (**1**), 6,6′-bis(chloromethyl)-2,2′-bipyrazine (**2**), and 6-(chloromethyl)-6′-methyl-2,2′-bipyrazine (**3**) were synthesized according to literature procedures.[8]

X-ray Data Collection and Processing: Crystals of Cl_2bpz were grown from hexane/Et_2O solution. Good quality specimens of the colourless parallelepiped-shaped crystals were chosen for X-ray diffraction analysis. They were placed on the goniometer head of an Enraf-Nonius CAD4 diffractometer, equipped with a liquid-nitrogen vapour stream low-temperature device and analyzed using Mo-K_α radiation (λ = 0.70931 Å). The diffractometer was housed in a Plexiglas box to protect it from atmospheric moisture and to avoid ice formation on the crystals. The temperature (110 ± 2 K) was monitored by a copper-constantan thermocouple positioned about 5 cm above the crystal. The first sample disintegrated within a few minutes in the nitrogen vapour stream, showing the fragility of these crystals upon cooling. A second crystal (0.2 × 0.3 × 0.4 mm) was then mounted on the diffractometer and the temperature was decreased in a more controlled manner. The orientation matrix and the unit cell parameters were determined by a least-squares fit to the optimized setting angles of 25 reflections in the Bragg angle range 20° ≤ 2θ ≤ 52°. The lattice parameters were determined as *a* = 5.145(2), *b* = 8.302(2), *c* = 12.320(3) Å, and β = 91.327(4)°. The relative variations of these parameters compared to room temperature values were evaluated as $\Delta a/a = 0.007$, $\Delta b/b = 0.02$, $\Delta c/c = 0.02$, and $\Delta V/V = 0.04$, respectively, where *V* is the unit cell volume. Inspection of the systematic intensity extinction revealed that the compound crystallizes in the $P2_1/n$ space group: no condition for (*hkl*) reflections, $k = 2n + 1$ for (0*k*0) and $h + l = 2n + 1$ for (*h*0*l*). The conditions and details of the diffraction experiment are presented in Table 5. A total of 21634 intensities were measured in the full reciprocal sphere ($-h$ to *h*, $-k$ to *k*, and $-l$ to *l*) and recorded as ω−2θ scan Bragg profiles up to a maximum resolution of $\sigma_{max} = (\sin\theta/\lambda)_{max} = 1.27$ Å^{-1}. During the data collection, three selected reflections (0 0 −6), (2 −5 −8), and (1 0 −13) were monitored every 2 h in order to check for variation of the intensities. The intensities of the (3 0 −1), (2 −5 −8), and (0 7 −8) reflections were measured every 200 reflections to check for any crystal disorientation. The total X-ray exposure time of the sample was 550 h and no temperature or crystal problems were observed during the experiment.

Data reduction and error analysis were performed using the D.R.E.A.D.D package of programs of Blessing.[28][29] A Lorentzian peak width model was used to determine the Bragg reflection limits and to integrate the intensity profiles. The instrumental instability coefficient based on the variation statistics of the standard reflection intensities was determined as π = 0.029(9). The variance of each observed intensity *I* was estimated as $\sigma^2(I) = [s^2_c(I) + (pI^2)^2]$, where $s^2_c(I)$ was calculated from the propagation of error based on counting statistics and scan angle uncertainties [σ(ω) = 0.005°]. In accordance with the low value of the absorption coefficient (μ = 0.59 mm^{-1}) and the sample dimensions, no absorption correction was applied. The merging and averaging of the data were performed in the 2/*m* point group, giving rise to 5344 unique observations [$I > 3\sigma(I)$] for use in the least-squares refinements. The statistical indices are given in Table 5.

Structure and Electron Density Refinements: The crystal structure was solved by direct methods using SHELXS-86[30] and refined with the least-squares program MOLLY.[31] The form factors of the carbon, nitrogen, and chlorine atoms were calculated from the wavefunctions of Clementi et al.[32] The form factors of the bound hydrogen atoms were taken from Stewart et al.[33] The anomalous dispersion coefficients were taken from the International Tables of Crystallography[34] in order to correct the form factors. The hydrogen atom positions were found by difference Fourier synthesis. The scale factor, the atomic coordinates, and the anisotropic thermal parameters U_{ij} of the non-H atoms were refined with all data. The scale factor was then fixed and new refinements of non-H atomic *xyz* and U_{ij} values were carried out with high Bragg angle observations ($\sin\theta/\lambda = 0.9$ Å^{-1}). The coordinates of hydrogen atoms were adjusted by imposing the average value found by neutron diffraction studies on the C−H distances (1.08 Å).[35] The isotropic secondary extinction effects were corrected using the formalism of Thornley et al.[36] with extinction of type 1 and a Lorentzian crystal mosaic distribution. The final extinction parameter value applied to the diffracted intensities amounted to $\gamma = 0.46(4) \times 10^{-4}$, which corresponds to a maximum intensity loss of 20% for the (0 1 3) reflection.

The electron density distribution in the molecular crystal of Cl_2bpz was determined using the Hansen-Coppens model.[31] Here, the electron density of each atom in the asymmetric unit is expressed as shown in Equation 1 where ρ_{core} and ρ_{val} are Hartree-Fock spherical core and valence densities, respectively; ρ_{val} is normalized to one electron so that the refined valence population parameter P_{val} gives the net atomic charge *q* with respect to the number N_{val} of electrons in the free atom valence orbitals, $q = N_{val} - P_{val}$.

In the program MOLLY,[31] the asymmetric unit is constrained to neutrality. The $y_{lm\pm}$ values are spherical harmonic angular functions of order *l* in real form, while $R_{nl}(r)$ are Slater-type radial functions $R_{nl}(r) = N_l r^{nl}\exp(-\zeta r)$, where N_l is the normalization factor, and n_l and ζ are parameters depending on the order *l* and the atomic valence functions, respectively.[37] P_{lm} are the multipole population parameters of each associated spherical harmonic function $y_{lm\pm}$. The coefficients κ and κ′ are related to the contraction or expansion of the electron density[38] for spherical and multipolar valence densities, respectively. In the Hansen-Coppens model,[31] the atomic electron density is expressed in local reference frames taking into account the chemical environment and the local symmetry. Figure 6 shows the local orthogonal axes chosen for the Cl_2bpz molecule. As in our previous study of Ph_2bpm, the multipolar expansion was truncated at the octupolar level for C, N, and Cl atoms ($l_{max} = 3$) and at the dipolar level ($l_{max} = 1$) for the hydrogen atoms. No significant occupation of higher multipole levels was observed. The radial functions of C, N, and H atoms were those of the previous study of Ph_2bpm,[16], i.e. $\zeta_C = 3.0$ bohr^{-1}, $\zeta_N = 3.8$ bohr^{-1}, $\zeta_H = 2.26$ bohr^{-1} (1 bohr = 0.529177 Å) and the multipole exponents were $n_l = 2,2,3$ for C and N up to the octupole level, and $n_l = 1$ for H, respectively. The best radial function for the chlorine atom was obtained by inspection of the residual maps:[39] $\zeta_{Cl} = 4.4$ bohr^{-1}, while the best exponents were found for $n_l = 6,6,6$. The number of multipolar parameters was reduced by imposing planar symmetry on the atomic electron densities of the pyrazine ring: All multipole populations associated with odd powers of *z* (Cartesian coordinate perpendicular to the plane) were not refined. A similar constraint was used in the electron study of the Ph_2bpm molecule. The final statistical indices for spherical and multipolar refinements are given in Table 6. Table 7 gives the atomic fractional coordinates and thermal parameters and their estimated standard deviations (e.s.d.′s) after the multipolar refinement. Hirshfeld's rigid bond test[40] gave a maximum value of 0.0005 Å^2 for the difference between the mean-squares displace-

Table 5. Experimental details of the X-ray data collection for 6,6′-bis(chloromethyl)-2,2′-bipyrazine

Crystal data:	
Empirical formula	$C_{10}H_8Cl_2N_4$
Molecular mass [g/mol]	255.1
Cell setting	monoclinic
Space group	*P*21/*n*
a [Å]	5.145(2)
b [Å]	8.302(2)
c [Å]	12.320(3)
β [°]	91.327(4)
V [Å^3]	526.09 (4)
Z	4
D_x [Mg m^{-3}]	1.543
Radiation type (graphite monochromator)	Mo-K_α
Wavelength [Å]	0.70931
No. of reflections for cell parameters	25
2θ range [°]	20−52
μ [mm^{-1}]	0.59
Temperature	110 K (liq. N_2 vapour stream)
Crystal form	parallelepiped
Crystal size [mm]	0.2 × 0.3 × 0.4
Crystal colour	colourless
Data collection:	
Diffractometer	Enraf-Nonius CAD-4
Data collection method	ω−2θ scans
Absorption correction	no
No. of measured reflections	21634
No. of used unique reflections	5344 [$I > 3\sigma(I)$]
*R*1, *R*2, R_w, S[a]	0.0277, 0.0277, 0.0582, 1.55
max [°]	64.3
Range of *h*, *k*, *l*	$-13 \le h \le 13$ $-21 \le k \le 21$ $-26 \le l \le 29$
No. of standard reflections	3
Frequency of standard reflections [min]	120
Intensity decay (%)	none

[a] The internal agreement factors are defined as : $R_1 = \dfrac{\sum_{\mathbf{H}} \sum_{i}^{N(\mathbf{H})} |I(\mathbf{H})_i - \overline{I(\mathbf{H})}|}{\sum_{\mathbf{H}} \sum_{i}^{N(\mathbf{H})} |I(\mathbf{H})_i|}$, $R_2 = \left[\dfrac{\sum_{\mathbf{H}} \sum_{i}^{N(\mathbf{H})} [I(\mathbf{H})_i - \overline{I(\mathbf{H})}]^2}{\sum_{\mathbf{H}} \sum_{i}^{N(\mathbf{H})} I(\mathbf{H})_i^2}\right]^{\frac{1}{2}}$,

$R_w = \left[\dfrac{\sum_{\mathbf{H}} \sum_{i}^{N(\mathbf{H})} w_i [I(\mathbf{H})_i - \overline{I(\mathbf{H})}]^2}{\sum_{\mathbf{H}} \sum_{i}^{N(\mathbf{H})} w_i I(\mathbf{H})_i^2}\right]^{\frac{1}{2}}$ $Z = \left[\dfrac{N_{measured} \sum_{\mathbf{H}} \sum_{i}^{N(\mathbf{H})} w_i^2 [I(\mathbf{H})_i - \overline{I(\mathbf{H})}]^2}{\{N_{measured} - N_{unique}\} \sum_{\mathbf{H}} \sum_{i}^{N(\mathbf{H})} w_i}\right]^{\frac{1}{2}}$,

the intensity $I(\mathbf{H}) = K^{-2}|F_O(\mathbf{H})|^2$ ($|F_O(\mathbf{H})|$ is the modulus of the observed structure factor and K^{-1}, its scale factor), $N_{measured} = \sum_{\mathbf{H}} N(\mathbf{H})$ and N_{unique} are the number of equivalent reflections and the number of unique reflections (with averaged intensity $\overline{I(\mathbf{H})}$) respectively and $w_i = \dfrac{1}{\sigma^2(I(\mathbf{H})_i)}$ is the statistical weight related to the diffraction intensity variance.

$$\rho_{at}(r) = \rho_c(r) + P_{val}\kappa^3\rho(\kappa r) + \sum_{l=0}^{l_{max}} \sum_{m=0}^{l} \kappa'^3 R_{nl}(\kappa' r) P_{lm} \pm y_{lm} \pm (\theta,\varphi) \qquad (1)$$

ment along the interatomic bonds for the N^1-C^4 and C^1-Cl linkages. This is lower than 0.001 Å^2, which is the limiting value of the test, and shows the excellent deconvolution between the atomic thermal displacement and the electron density in the molecular bonds. After the multipolar refinement, the maximum residual electron density does not exceed 0.1 eÅ^{-3} in the plane of the pyrazine ring, as shown in Figure 7. Some peaks reaching 0.2 eÅ^{-3} remain around the chlorine atom; the corresponding residual electron den-

sity map has been deposited as supplementary material. These values are satisfactory when compared with the estimation of experimental errors according to Equation 2,[41,42] where $|F_{obs}(\mathbf{H})|$ and $|F_{calc}(\mathbf{H})|$ are the moduli of observed and calculated structure factor, respectively, at the Bragg vector H, K^{-1} is the scale factor, and V is the unit cell volume.

$$\langle\sigma^2(\Delta\rho)\rangle^{1/2} = \frac{2}{V_{cell}}\left[\sum_{H}(\sigma^2(K^{-1}|F_{obs}(H)|)\right]^{1/2} = 0.06\ e\text{Å}^{-3} \text{ and}$$

$$\langle\sigma^2_{res}\rangle^{1/2} = \frac{2}{V_{cell}}\left[\sum_{H}(K^{-1}|F_{obs}(H)| - |F_{calc}(H)|)^2\right]^{1/2} = 0.05\ e\text{Å}^{-3} \quad (2)$$

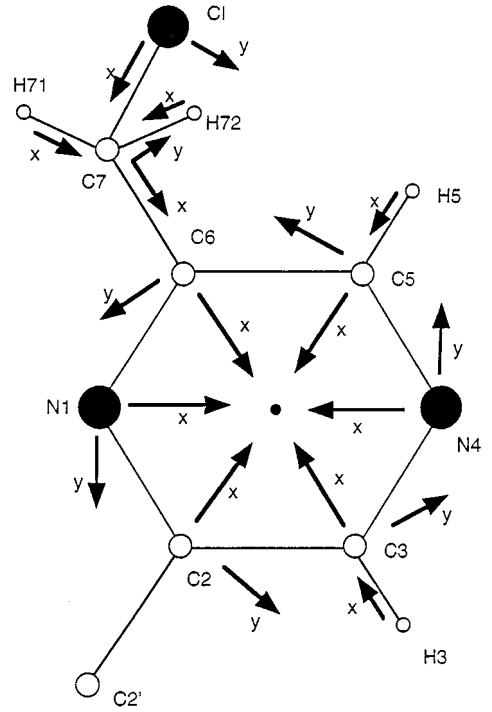

Figure 6. Local atomic frames for the electron density multipolar expansion

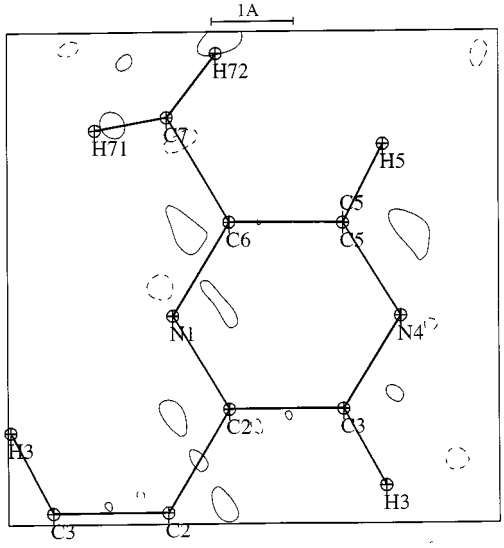

Figure 7. Residual density in the pyrazine ring of the 6,6′-bis(chloromethyl)-2,2′-bipyrazine molecule; contour intervals ±0.1 eÅ^{-3}; negative contours are dashed, zero contour omitted

6-(Hydroxymethyl)-6′-methyl-2,2′-bipyrazine (4) and 3-Hydroxy-6,6′-dimethyl-2,2′-bipyrazine (5). − Method A: A solution of Na_2CO_3 (1.92 g, 18.1 mmol) in water (10 mL) was added to a solution of 6-(chloromethyl)-6′-methyl-2,2′-bipyrazine (**3**) (0.50 g, 2.26 mmol) in CH_3CN (15 mL) and the resulting mixture was stirred for 24 h at 70°C. After evaporation of the solvent, the concentrated aqueous solution was neutralized with conc. HCl and extracted with $CHCl_3$ (2 × 20 mL). The combined organic phases were dried with anhydrous $MgSO_4$ and the solvent was evaporated. The solid residue was purified by column chromatography (elution: CH_2Cl_2/MeOH) to provide pure **4** (0.214 g, 47%) and **5** (0.080 g, 17.5%) as white powders.

Method B: A solution of 6-(chloromethyl)-6′-methyl-2,2′-bipyrazine (**3**) (0.030 g, 0.13 mmol) in CH_3CN (15 mL) was heated with 1 N aq. NaOH (5 mL) for 24 h at 60°C. After cooling, the acetonitrile was evaporated and the concentrated aqueous solution was extracted with $CHCl_3$ (2 × 20 mL). The combined organic phases were dried with anhydrous $MgSO_4$ and the solvent was evaporated. The solid residue was purified by column chromatography (elution: CH_2Cl_2/MeOH) to provide **4** (7 mg, 25%) and **5** (4 mg, 14%) as pure white powders.

4: TLC (CH_2Cl_2/MeOH, 90:10): R_f = 0.4. − ^{1}H NMR ($CDCl_3$): δ = 9.45 (s, 1 H), 9.31 (s, 1 H), 8.64 (s, 1 H), 8.47 (s, 1 H), 4.87 (s, 2 H), 2.60 (s, 3 H). − MS (70 eV); *m*/*z*: 202 [M$^{+\cdot}$], 201, 186, 173. − $C_{10}H_{10}N_4O$ (202): calcd. C 59.40, H 4.95, N 27.72; found C 59.55, H 4.97, N 28.00.

5: TLC (CH_2Cl_2/MeOH, 90:10): R_f = 0.5. − ^{1}H NMR ($CDCl_3$): δ = 9.59 (s, 1 H), 8.51 (s, 1 H), 8.07 (s, 1 H), 2.60 (s, 3 H), 2.49 (s, 3 H). − MS (70 eV); *m*/*z*: 202 [M$^{+\cdot}$], 174. − $C_{10}H_{10}N_4O$ (202): calcd. C 59.40, H 4.95, N 27.72; found C 59.62, H 4.99, N 27.95.

6-(Methoxymethyl)-6′-methyl-2,2′-bipyrazine (6), 3-Methoxy-6,6′-dimethyl-2,2′-bipyrazine (7), and 5-Methoxy-6,6′-dimethyl-2,2′-bipyrazine (8). − Method A: A solution of NaOH (0.4 N, 1 mL) in MeOH (3 mL) was added to a solution of **3** (0.10 g, 0.45 mmol) in MeOH (5 mL) and the resulting mixture was stirred for 24 h at room temperature. After evaporation of the solvent, the residue was extracted with 20 mL of chloroform and the organic layer was dried with anhydrous $MgSO_4$. After concentration to dryness, the residue was purified by column chromatography (elution: toluene/ethyl acetate) to provide **6** (29 mg, 29.6%), **7** (12 mg, 12.3%), and **8** (20 mg, 20.4%) as pure white powders.

Method B: Under argon, **3** (0.23 g, 1.04 mmol) was added to a sodium methanolate solution prepared from sodium (0.015 g, 0.65 mmol) and MeOH (15 mL). The reaction was allowed to proceed for 8 h at room temperature. The solvent was then evaporated and the residue was purified by column chromatography (elution: hexane/ethyl acetate) to provide **6** (0.133 g, 59%), **7** (0.047 g, 20.6%), and **8** (0.046 g, 20.4%) as pure white powders.

6: TLC (toluene/ethyl acetate, 40:60): R_f = 0.37. − ^{1}H NMR ($CDCl_3$): δ = 9.46 (s, 1 H), 9.33 (s, 1 H), 8.73 (s, 1 H), 8.48 (s, 1 H), 4.69 (s, 2 H), 3.52 (s, 3 H), 2.62 (s, 3 H). − MS (70 eV); *m*/*z*: 216 [M$^{+\cdot}$], 186. − $C_{11}H_{12}N_4O$ (216): calcd. C 61.11, H 5.55, N 25.92; found C 61.21, H 5.57, N 26.01.

7: TLC (toluene/ethyl acetate, 40:60): R_f = 0.22. − ^{1}H NMR ($CDCl_3$): δ = 8.91 (s, 1 H), 8.41 (s, 1 H), 7.99 (s, 1 H), 3.95 (s, 3 H), 2.62 (s, 3 H), 2.53 (s, 3 H). − MS (70 eV); *m*/*z*: 216 [M$^{+\cdot}$], 199, 187. − $C_{11}H_{12}N_4O$ (216): calcd. C 61.11, H 5.55, N 25.92; found C 61.31, H 5.50, N 26.03.

8: TLC (toluene/ethyl acetate, 40:60): R_f = 0.60. − ^{1}H NMR ($CDCl_3$): δ = 9.17 (s, 1 H), 8.83 (s, 1 H), 8.34 (s, 1 H), 3.97 (s, 3

Table 6. Least-squares statistical factors R, R_w and *g.o.f.* of the refinement strategies

$s = (\sin\theta)/\lambda$ [Å^{-1}]	R[a] (%)	R_w[a] (%)	*g.o.f.* [a]	n[a]	m[a]	Type of refinement
$0.0 \le s \le 1.27$	3.21	4.77	1.61	74	5344	Spherical all data
$0.9 \le s \le 1.27$	4.48	4.93	1.15	72	2599	Spherical high order data
$0.0 \le s \le 1.27$	3.26	4.96	1.66	2	5344	Spherical all data
$0.0 \le s \le 1.27$	2.51	3.18	1.09	202	5344	Multipolar all data

[a] $R(F) = \frac{\sum_{\mathbf{H}} | K^{-1}|F_o(\mathbf{H})| - |F_c(\mathbf{H})| |}{\sum_{\mathbf{H}} K^{-1}|F_o(\mathbf{H})|}$, $R_w(F) = \left[\frac{\sum_{\mathbf{H}} w_{\mathbf{H}} [K^{-1}|F_o(\mathbf{H})| - |F_c(\mathbf{H})|]^2}{\sum_{\mathbf{H}} w_{\mathbf{H}} K^{-2}|F_o(\mathbf{H})|^2} \right]^{\frac{1}{2}}$ g.o.f. $= \left[\frac{1}{m-n} \sum_{\mathbf{H}} w_{\mathbf{H}} [K^{-1}|F_o(\mathbf{H})| - |F_c(\mathbf{H})|]^2 \right]^{\frac{1}{2}}$

where $|F_O(\mathbf{H})|$ and $|F_C(\mathbf{H})|$ are the moduli of the observed and the calculated structure factor respectively, $w_{\mathbf{H}} = \frac{1}{\sigma^2(|F_O(\mathbf{H})|)}$ is the statistical weight, K^{-1} is the scale factor, n is the number of refined parameters and m the number of data.

Table 7. Fractional atomic coordinates and anisotropic thermal parameters U^{ij} [Å^2]

	x	y	z
N4	0.46452(8)	0.80464(5)	−0.07385(3)
N1	0.09672(7)	0.83659(4)	0.08823(3)
C7	0.27082(9)	0.60609(5)	0.18593(3)
C6	0.27986(8)	0.72241(4)	0.09347(3)
C5	0.46849(8)	0.71048(5)	0.01417(3)
C3	0.27676(8)	0.91508(5)	−0.08041(2)
C2	0.09719(7)	0.93462(4)	0.00235(3)
Cl	0.01860(2)	0.45916(1)	0.15825(1)
H7	0.22167	0.67744	0.25543
H7	0.46255	0.55648	0.19788
H5	0.61646	0.62027	0.02631
H3	0.26180	0.99150	−0.15081

	$U11$	$U22$	$U33$	$U12$	$U13$	$U23$[a]
N4	0.0143(1)	0.0138(1)	0.0133(1)	0.0024(1)	0.0043(1)	0.0008(1)
N1	0.0130(1)	0.0119(1)	0.0103(1)	0.0017(1)	0.0018(1)	0.0016(1)
C7	0.0158(1)	0.0138(1)	0.0118(1)	0.0008(1)	−0.0011(1)	0.0023(1)
C6	0.0125(1)	0.0111(1)	0.0108(1)	0.0008(1)	0.0006(1)	0.0009(1)
C5	0.0130(1)	0.0119(1)	0.0138(1)	0.0017(1)	0.0022(1)	0.0003(1)
C3	0.0142(1)	0.0132(1)	0.0109(1)	0.0015(1)	0.0030(1)	0.0013(1)
C2	0.0114(1)	0.0106(1)	0.0099(1)	0.0006(1)	0.0013(1)	0.0006(1)
Cl	0.01801(1)	0.01205(3)	0.01382(3)	−0.00063(3)	0.00152(2)	0.00143(2)
H71	0.029(6)					
H72	0.042(5)					
H5	0.031(5)					
H3	0.028(5)					

[a] $T(\mathbf{H}) = \exp -2\pi^2 \sum_{i,j=1}^{3} U^{ij} h_i h_j a_i^* a_j^*$ is the temperature factor where a_i^*'s are the reciprocal space unit cell parameters and h_i are the **H** Bragg vector components; estimated standard deviations are given in parentheses.

H), 2.54 (s, 3 H), 2.48 (s, 3 H). − MS (70 eV); *m/z*: 216 [$M^{+\cdot}$], 201, 187. − $C_{11}H_{12}N_4O$ (216): calcd. C 61.11, H 5.55, N 25.92; found C 61.05, H 5.49, N 25.82.

6-(2-Hydroxyethyloxymethyl)-6′-methyl-2,2′-bipyrazine (9), 3-(2-Hydroxyethyloxy)-6,6′-dimethyl-2,2′-bipyrazine (10), and 5-(2-Hydroxyethyloxy)-6,6′-dimethyl-2,2′-bipyrazine (11). − Method A: A suspension of **3** (0.029 g, 0.13 mmol) in ethylene glycol (10 mL) was heated with NaOH (2 N, 2 mL) until a clear solution was obtained, which was then stirred for a further 72 h. After cooling and evaporation of the solvent, the residue was purified by column chromatography. Two separations were needed, the first (elution: ethyl acetate/hexane) to separate pure **10** (2 mg, 6%) and the second (elution: CH_2Cl_2/MeOH) to separate **9** (18 mg, 53%) and **11** (2 mg, 6%).

Method B: Under argon, **3** (0.104 g, 0.47 mmol) was added to a solution of sodium ethylene glycolate, prepared from ethylene glycol (10 mL) and sodium (0.025 g, 1.08 mmol), and the reaction mixture was stirred for 45 h at room temperature. The solution was

then hydrolysed by the addition of distilled water (10 mL), neutralized with 5% aq. HCl, extracted with CH_2Cl_2 (2 × 50 mL), and the combined organic phases were dried with anhydrous $MgSO_4$. After evaporation of the solvent, the residue was purified by column chromatography under the same conditions as described in Method A, to give pure **10** (21 mg, 18%), **9** (48 mg, 41%), and **11** (20 mg, 17%).

9: TLC (CH_2Cl_2/MeOH, 90:10): R_f = 0.45. − ^{1}H NMR ($CDCl_3$): δ = 9.42 (s, 1 H), 9.27 (s, 1 H), 8.70 (s, 1 H), 8.45 (s, 1 H), 4.75 (s, 2 H), 3.79 (m, 2 H), 3.72 (m, 2 H), 2.58 (s, 3 H). − MS (70 eV); *m*/*z*: 247 [$M^{+\cdot}$ + H^+], 201, 186. − $C_{12}H_{14}N_4O_2$ (246): calcd. C 58.53, H 5.69, N 22.76; found C 58.41, H 5.71, N 22.91.

10: TLC (hexane/ethyl acetate, 90:10): R_f = 0.10. − ^{1}H NMR ($CDCl_3$): δ = 8.98 (s, 1 H), 8.45 (s, 1 H), 8.00 (s, 1 H), 4.53 (m, 2 H), 3.85 (m, 2 H), 2.59 (s, 3 H), 2.52 (s, 3 H). − MS (70 eV); *m*/*z*: 246 [$M^{+\cdot}$], 216, 187, 173. − $C_{12}H_{14}N_4O_2$ (246): calcd. C 58.53, H 5.69, N 22.76; found C 58.61, H 5.67, N 22.93.

11: TLC (hexane/ethyl acetate, 90:10): R_f = 0.15. − ^{1}H NMR ($CDCl_3$): δ = 9.19 (s, 1 H), 8.81 (s, 1 H), 8.36 (s, 1 H), 4.52 (m, 2 H), 3.96 (m, 2 H), 2.55 (s, 3 H), 2.52 (s, 3 H). − MS (70 eV); *m*/*z*: 246 [$M^{+\cdot}$], 216, 187, 173. − $C_{12}H_{14}N_4O_2$ (246): calcd. C 58.53, H 5.69, N 22.76; found C 58.65, H 5.72, N 22.87.

6′-Methyl-6-(4-nitrophenyloxymethyl)-2,2′-bipyrazine (12) and 6′-Methyl-3-(4-nitrophenyloxy)-2,2′-bipyrazine (13): Sodium *p*-nitrophenolate was first prepared from *p*-nitrophenol (0.050 g, 0.35 mmol) and sodium (0.100 g, 4.3 mmol) in anhydrous EtOH (20 mL). After evaporation of the solvent, the product was added to a solution of **3** (0.049 g, 0.22 mmol) in anhydrous CH_3CN (15 mL) under argon. The resulting mixture was stirred for 48 h at 70°C. After cooling, the solvent was evaporated and the residue was purified by column chromatography (elution: CH_2Cl_2/MeOH) to provide **12** and **13** as yellow-orange powders.

12: Yield: 0.025 g (35%). − TLC (CH_2Cl_2/MeOH, 95:5): R_f = 0.75. − ^{1}H NMR ($CDCl_3$): δ = 9.51 (s, 1 H), 9.30 (s, 1 H), 8.79 (s, 1 H), 8.48 (s, 1 H), 8.18 (d, 2 H), 7.06 (d, 2 H), 5.35 (s, 2 H), 2.60 (s, 3 H). − MS (70 eV); *m*/*z*: 323 [$M^{+\cdot}$], 185, 66. − $C_{16}H_{13}N_5O_3$ (323): calcd. C 59.44, H 4.02, N 21.67; found C 59.22, H 4.05, N 21.86.

13: Yield: 0.009 g (12.5%). − TLC (CH_2Cl_2/MeOH, 95:5): R_f = 0.45. − ^{1}H NMR ($CDCl_3$): δ = 10.19 (s, 1 H), 9.76 (s, 1 H), 9.15 (s, 1 H), 7.60 (m, 2 H), 7.40 (m, 2 H), 2.85 (s, 3 H), 2.63 (s, 3 H). − MS (70 eV); *m*/*z*: 323 [$M^{+\cdot}$], 277. − $C_{16}H_{13}N_5O_3$ (323): calcd. C 59.44, H 4.02, N 21.67; found C 59.35, H 4.01, N 21.81.

6,6′,6′′′-Trimethyl-3′,6′′-(oxymethylene)bis(2,2′-bipyrazine) (14): To a solution of **4** (0.033 g, 0.16 mmol) in anhydrous THF (16 mL) under argon at 0°C was added NaH (0.005 g, 0.2 mmol). After stirring for 30 min at 0°C, **3** (0.036 g, 0.16 mmol) was added in a single portion and the reaction was allowed to proceed for 20 h at 50°C. After cooling, distilled water (20 mL) was carefully added. The aqueous phase was extracted with CH_2Cl_2 (2 × 20 mL) and the combined organic extracts were dried with $MgSO_4$. Evaporation of the solvent left a solid, which was purified by column chromatography (elution: CH_2Cl_2/MeOH) to provide **14** (6 mg, 10%). − TLC (CH_2Cl_2/MeOH, 90:10): R_f = 0.46. − ^{1}H NMR ($CDCl_3$): δ = 9.48 (s, 1 H), 9.33 (s, 1 H), 9.21 (s, 1 H), 8.86 (s, 1 H), 8.77 (s, 1 H), 8.47 (s, 1 H), 8.37 (s, 1 H), 5.67 (s, 2 H), 2.61 (s, 6 H), 2.55 (s, 3 H). − MS (70 eV); *m*/*z*: 386 [$M^{+\cdot}$], 201, 186. − $C_{20}H_{18}N_8O$ (386): calcd. C 62.17, H 4.66, N 29.02; found C 62.25, H 4.68, N 29.12.

6-(Chloromethyl)-6′,6′′′-dimethyl-3′,6′′-(oxymethylene)bis(2,2′-bipyrazine) (15) and 6-(Chloromethyl)-6′,6′′′-dimethyl-5′,6′′-(oxymethylene)bis(2,2′-bipyrazine) (16): NaH (0.012 g, 0.5 mmol) was added to a solution of **4** in anhydrous THF (40 mL) at 0°C. The resulting suspension was stirred vigorously for 1 h, **2** (0.034 g, 0.13 mmol) was then added, and the reaction mixture was heated at 50°C for 24 h. After cooling, water (10 mL) was carefully added, the resulting solution was extracted with $CHCl_3$ (2 × 20 mL), and the combined organic extracts were dried with anhydrous $MgSO_4$. Evaporation of the solvent left a solid, which was purified by column chromatography (elution: CH_2Cl_2/MeOH) to provide **15** and **16** as pale-yellow powders.

15: Yield: 0.010 g (21%). − TLC (CH_2Cl_2/MeOH, 90:10): R_f = 0.6. − ^{1}H NMR ($CDCl_3$): δ = 9.49 (s, 1 H), 9.39 (s, 1 H), 9.32 (s, 1 H), 8.89 (s, 1 H), 8.77 (s, 1 H), 8.66 (s, 1 H), 8.47 (s, 1 H), 5.67 (s, 2 H), 4.68 (s, 2 H), 2.61 (s, 3 H), 2.60 (s, 3 H). − MS (70 eV); *m*/*z*: 420 [$M^{+\cdot}$], 384, 201, 186. − $C_{20}H_{17}ClN_8O$ (420): calcd. C 57.14, H 4.04, Cl 8.45, N 26.66; found C 57.21, H 4.08, Cl 8.25, N 26.75.

16: Yield: 0.015 g (31%). − TLC (CH_2Cl_2/MeOH, 90:10): R_f = 0.5. − ^{1}H NMR ($CDCl_3$): δ = 9.46 (s, 1 H), 9.29 (s, 1 H), 9.20 (s, 1 H), 8.81 (s, 1 H), 8.75 (s, 1 H), 8.46 (s, 1 H), 8.03 (s, 1 H), 5.66 (s, 2 H), 4.77 (s, 2 H), 2.59 (s, 3 H), 2.55 (s, 3 H). − MS (70 eV); *m*/*z*: 420 [$M^{+\cdot}$], 384, 355, 293, 249, 235, 201, 186. − $C_{20}H_{17}ClN_8O$ (420): C 57.14, H 4.04, Cl 8.45, N 26.66; found C 57.17, H 4.07, Cl 8.22, N 26.49.

6-(Aminomethyl)-6′-methyl-2,2′-bipyrazine (17): A solution of **3** (0.320 g, 1.47 mmol) in CH_2Cl_2 (10 mL) was added to a solution of hexamethylenetetraamine (0.230 g, 1.64 mmol) in CH_2Cl_2 (10 mL) under reflux. The reaction mixture was subsequently stirred for 6 h. A white solid was deposited during the course of the reaction, which was filtered off, dried, and taken up in hot EtOH (7 mL) acidified with conc. HCl (1 mL). The resulting suspension was stirred at 80°C until a clear solution was obtained (24 h). After cooling, the solvent was evaporated and water (2 mL) was added to the residue. The aqueous phase was made alkaline with 10 M aq. KOH and then extracted with CH_2Cl_2 (2 × 25 mL). The combined organic phases were dried with $MgSO_4$ and the solvent was evaporated to leave **17** as a white powder. Yield: 0.108 g (37%). − TLC (CH_2Cl_2/MeOH, 95:5): R_f = 0.1. − ^{1}H NMR ($CDCl_3$): δ = 9.39 (s, 1 H), 9.33 (s, 1 H), 8.57 (s, 1 H), 8.45 (s, 1 H), 4.05 (s, 2 H), 2.59 (s, 3 H), 1.75 (s, 2 H). − M.p. 129°C. − MS (70 eV); *m*/*z*: 201 [$M^{+\cdot}$], 186, 173, 144. − $C_{10}H_{11}N_5$ (201): calcd. C 59.70, H 5.47, N 34.82; found C 59.58, H 5.43, N 34.58.

6,6′-Bis(azidomethyl)-2,2′-bipyrazine (18): To a solution of sodium azide (0.283 g, 4.35 mmol) in DMSO (10 mL) at 70°C, **2** (0.19 g, 0.74 mmol) was added portionwise. The reaction mixture was maintained at 70°C for a further 2 h. After cooling, distilled water (10 mL) was added and the aqueous phase was extracted with toluene (2 × 20 mL). The combined organic extracts were dried with anhydrous $MgSO_4$ and the solvent was evaporated. The residue was purified by column chromatography (elution: CH_2Cl_2/MeOH) to furnish **18** as a white powder. Yield: 0.145 g (77%). − TLC (toluene/ethyl acetate, 50:50): R_f = 0.48. − ^{1}H NMR ($CDCl_3$): δ = 9.58 (s, 2 H), 8.70 (s, 2 H), 4.60 (s, 4 H). − MS (70 eV); *m*/*z*: 268 [$M^{+\cdot}$], 197, 196. − $C_{10}H_8N_{10}$ (268): calcd. C 44.77, H 2.98, N 52.23; found C 44.80, H 2.97, N 52.11.

6,6′-Bis(aminomethyl)-2,2′-bipyrazine (19): To a solution of **18** (0.078 g, 0.29 mmol) in CH_2Cl_2/EtOH (1:3) (10 mL) was added 10% Pd/C (0.012 g). The reaction mixture was stirred under H_2 at a pressure of 5 bar for 6 h, then filtered through Celite, and the catalyst was washed with CH_2Cl_2. The solvent was evaporated from the combined filtrate and washings, and the residue was treated with 5% aq. HCl (5 mL). The resulting acidic aqueous phase was extracted with CH_2Cl_2, then neutralized with Na_2CO_3 and ex-

tracted with further CH_2Cl_2 (3 × 20 mL). The combined organic extracts were dried with anhydrous $MgSO_4$. After evaporation of the solvent, **19** was obtained as a white powder. Yield: 0.031 g (48%). − TLC (CH_2Cl_2/MeOH, 95:5): R_f = 0.1. − ^{1}H NMR ($CDCl_3$): δ = 9.41 (s, 2 H), 8.60 (s, 2 H), 4.07 (s, 4 H), 1.77 (s, 4 H). − MS (70 eV); *m/z*: 216 [M^+], 199, 188. − $C_{10}H_{12}N_6$ (216): calcd. C 55.55, H 5.55, N 38.88; found C 55.61, H 5.52, N 39.02.

6,6′-Bis(thiomethyl)-2,2′-bipyrazine (20): A solution of **2** (0.045 g, 0.17 mmol) and thiourea (0.040 g, 0.52 mmol) in acetone (10 mL) was stirred under reflux for 24 h. After cooling and evaporation of the solvent, the crude solid was washed with diethyl ether (3 × 10 mL), collected by filtration, and placed in a dessicator over night. The dry powder was subsequently dissolved in a mixture of 2 mL of $CHCl_3$ and 1 mL of MeOH and the resulting solution was poured into a solution of $K_2S_2O_5$ (0.078 g, 0.35 mmol) in water (1 mL). The mixture was stirred under reflux for a further 2 h. After cooling, 2 mL of water was added and the mixture was extracted with $CHCl_3$ (2 × 20 mL). The combined organic extracts were dried with anhydrous $MgSO_4$. After evaporation of the solvent, **20** was obtained as a pale-yellow powder. Yield: 0.037 g (84%). − TLC (CH_2Cl_2/MeOH, 95:5): R_f = 0.18. − ^{1}H NMR ($CDCl_3$): δ = 9.41 (s, 2 H), 8.63 (s, 2 H), 3.89 (s, 4 H). − MS (70 eV); *m/z*: 250 [M^+], 218, 144. − $C_{10}H_{10}N_4S_2$ (250): calcd. C 48.00, H 4.00, N 22.40, S 25.60; found C 48.11, H 4.02, N 22.21, S 25.34.

6′-Methyl-6-methylthio-2,2′-bipyrazine (21): A solution of **3** (0.025 g, 0.11 mmol) and thiourea (0.014 g, 0.18 mmol) in acetone (10 mL) was stirred under reflux for 24 h. After cooling and evaporation of the solvent, the crude solid was washed with diethyl ether (3 × 10 mL), collected by filtration, and placed in a dessicator for one night. The dry powder was subsequently dissolved in a mixture of 1 mL of $CHCl_3$ and 0.5 mL of MeOH, and the resulting solution was poured into a solution of $K_2S_2O_5$ (0.038 g, 0.17 mmol) in water (0.2 mL). The mixture was stirred under reflux for a further 1 h. After cooling, 2 mL of water was added and the mixture was extracted with $CHCl_3$ (2 × 20 mL). The combined organic extracts were dried with anhydrous $MgSO_4$. After evaporation of the solvent, **21** was obtained as a powder. Yield: 0.022 g (86%). − TLC (CH_2Cl_2/MeOH, 95:5): R_f = 0.35. − ^{1}H NMR ($CDCl_3$): δ = 9.35 (s, 1 H), 9.32 (s, 1 H), 8.61 (s, 1 H), 8.46 (s, 1 H), 3.90 (d, 2 H), 2.58 (s, 3 H). − MS (70 eV); *m/z*: 218 [M^+], 185, 144. − $C_{10}H_{10}N_4S$ (218): calcd. C 55.04, H 4.58, N 25.68, S 14.68; found C 55.12, H 4.60, N 25.29, S 14.58.

6,6′′-[(2,2′-Bipyrazin-6,6′-diyl)bis(methyleneoxymethylene)]-6′,6′′′-dimethylbis(2,2′-bipyrazine) (22): NaI (0.123 g, 0.82 mmol) was added to a solution of **2** (0.105 g, 0.41 mmol) in anhydrous THF (30 mL) and the resulting mixture was stirred under argon at room temperature for 4 h, whereupon a yellow-orange color appeared. At the same time, another solution was prepared from **4** (0.250 g, 1.23 mmol) and NaH (0.060 g, 2.5 mmol) in anhydrous THF (60 mL) under argon at 0°C. After allowing this solution to warm to room temperature, it was added to the first solution and the resulting mixture was stirred for a further 72 h. The reaction was subsequently quenched by the careful addition of distilled water (20 mL) and the resulting solution was extracted with CH_2Cl_2 (2 × 20 mL). The combined organic extracts were dried with anhydrous $MgSO_4$, the solvent was evaporated, and the residue was purified by column chromatography (elution: CH_2Cl_2/MeOH) to provide pure **21** (9 mg, 4%) and a by-product identified as pure dimer **15** (12 mg). − TLC (CH_2Cl_2/MeOH, 90:10): R_f = 0.4. − ^{1}H NMR ($CDCl_3$): δ = 9.49 (s, 2 H), 9.47 (s, 2 H), 9.31 (s, 2 H), 8.81 (s, 2 H), 8.76 (s, 2 H), 8.46 (s, 2 H), 4.93 (s, 6 H), 4.72 (s, 2 H), 2.60 (s, 6 H). − MS (70 eV); *m/z*: 586 [M^+], 570. − $C_{30}H_{26}N_{12}O_2$ (586): calcd. C 61.43, H 4.43, N 28.66; found C 61.51, H 4.45, N 28.53.

Acknowledgments

The CNRS and the University Henri Poincaré, Nancy-1, are acknowledged for their financial and technical support.

[1] [1a] B. Alpha, J.-M. Lehn, G. Mathis, *Angew. Chem. Int. Ed. Engl.* **1987**, *26*, 266−267. − [1b] B. Alpha, E. Anklam, R. Deschenaux, J.-M. Lehn, M. Pietraszkiewicz, *Helv. Chim. Acta* **1988**, *71*, 1042−1051. − [1c] R. Ziessel, J.-M. Lehn, *Helv. Chim. Acta* **1990**, *73*, 1149−1161. − [1d] J.-C. Rodriguez-Ubis, R. Sedano, G. Barroso, O. Juanes, E. Brunet, *Helv. Chim. Acta* **1997**, *80*, 86−96.
[2] [2a] H. Sleiman, P. Baxter, J.-M. Lehn, K. Rissanen, *J. Chem. Soc., Chem. Commun.* **1995**, 715−716. − [2b] R. Ziessel, M.-T. Youinou, *Angew. Chem. Int. Ed. Engl.* **1993**, *32*, 877−880.
[3] [3a] M. M. Harding, U. Koert, J.-M. Lehn, A. Marquis-Rigault, C. Piguet, J. S. Siegel, *Helv. Chim. Acta* **1991**, *74*, 594−610. − [3b] V. C. M. Smith, J.-M. Lehn, *J. Chem. Soc., Chem. Commun.* **1996**, 2733−2734. − [3c] B. Hasenknopf, J.-M. Lehn, B. O. Kneisel, G. Baum, D. Fenske, *Angew. Chem. Int. Ed. Engl.* **1996**, *35*, 1838−1840. − [3d] C. R. Woods, M. Benaglia, F. Cozzi, J. S. Siegel, *Angew. Chem. Int. Ed. Engl.* **1996**, *35*, 1830−1833.
[4] P. N. J. Baxter, J.-M. Lehn, J. Fischer, M.-T. Youinou, *Angew. Chem. Int. Ed. Engl.* **1994**, *33*, 2284−2286.
[5] P. N. J. Baxter, G. S. Hanan, J.-M. Lehn, *J. Chem. Soc., Chem. Commun.* **1996**, 2019−2020.
[6] J.-M. Lehn, J.-B. Regnouf de Vains, *Helv. Chim. Acta* **1992**, *75*, 1221−1236.
[7] [7a] A.-L. Papet, Ph. D. Dissertation, Univ. of Nancy, **1993**. − [7b] A.-L. Papet, A. Marsura, *Synthesis* **1993**, 478−481. − [7c] J.-B. Regnouf de Vains, J.-M. Lehn, N. E. Ghermani, Y. Dusausoy, A.-L. Papet, A. Marsura, P. Friant, J.-L. Rivail, *New J. Chem.* **1994**, *18*, 701−708. − [7d] F. Bodar-Houillon, T. Humbert, A. Marsura, J.-B. Regnouf de Vains, O. Dusausoy, N. Bouhmaida, N. E. Ghermani, Y. Dusausoy, *Inorg. Chem.* **1995**, *34*, 5205−5209.
[8] F. Bodar-Houillon, A. Marsura, *Tetrahedron Lett.* **1995**, *36*, 865−868.
[9] F. Bodar-Houillon, A. Marsura, *New J. Chem.* **1996**, *20*, 1041−1045.
[10] F. Bodar-Houillon, A. Marsura, *Supramol. Chem.* **1998**, *9*, 191−198.
[11] J.-B. Regnouf de Vains, R. Lamartine, *Helv. Chim. Acta* **1994**, *77*, 1817−1825.
[12] IUPAC designations are $1/D_N + 3/A_N$ or $1/D_N + 5/A_N$.
[13] J. March, *Advanced Organic Chemistry*, 4th ed., Wiley-Interscience, New York, **1992**, p. 328.
[14] For a review of the S_N2' mechanism, see: R. M. Magid, *Tetrahedron* **1980**, *36*, 1901.
[15] C. K. Johnson, *ORTEP*, Report ORNL-3794, 2nd revision, Oak Ridge National Laboratory, Oak Ridge, TN, **1970**.
[16] N. E. Ghermani, N. Bouhmaida, C. Lecomte, A.-L. Papet, A. Marsura, *J. Phys. Chem.* **1994**, *98*, 6287−6292.
[17] G. De With, S. Harkema, D. Feil, *Acta Crystallogr.* **1976**, *B32*, 3178−3184.
[18] T. Koritsanszky, M. K. Strumpel, J. Bushmann, P. Luger, N. K. Hansen, V. Pichon-Pesme, *J. Am. Chem. Soc.* **1991**, *113*, 9148−9154.
[19] N. E. Ghermani, N. Bouhmaida, C. Lecomte, ELECTROS, STATDENS: *Computer Programs to Calculate Electrostatic Properties from High-Resolution X-ray Diffraction Data*, Internal report URA CNRS 809, Univ. Henri Poincaré, Nancy-1, **1992**.
[20] M. Souhassou, C. Lecomte, N. E. Ghermani, M. M. Rohmer, R. Wiest, M. Bénard, R. H. Blessing, *J. Am. Chem. Soc.* **1992**, *114*, 2371−2382.
[21] V. Pichon-Pesme, C. Lecomte, H. Lachekar, *J. Phys. Chem.* **1995**, *99*, 6242−6250.
[22] G. Moss, D. Feil, *Acta Crystallogr.* **1981**, *A37*, 414−421.
[23] R. F. W. Bader, *Atoms in Molecules: A Quantum Theory*, International series of monographs on chemistry (Eds.: J. Halpen, M. L. H. Green), Clarendon Press, Oxford, **1990**.

[24] M. Souhassou, *Am. Cryst. Ass. Meet. Pittsburgh*, Pennsylvania, Abstract F06, August **1992**; *PROP: Computer Program to Calculate the Experimental Multipolar Electron Density from High-Resolution X-ray Diffraction Data*, Hauptman Woodward Institute (Buffalo, USA) and Internal Report URA CNRS 809, Université Henri Poincaré, Nancy-1, **1992**.
[25] A.-L. Papet, A. Marsura, N. E. Ghermani, C. Lecomte, P. Friant, J.-L. Rivail, *New J. Chem.* **1993**, *17*, 181−185.
[26] Y. Aray, R. F. W. Bader, *Surface Sci.* **1996**, 233−249.
[27] J.-B. Regnouf de Vains, A.-L. Papet, A. Marsura, *J. Heterocycl. Chem.* **1994**, *31*, 1069−1077.
[28] R. H. Blessing, *Crystallogr. Rev.* **1987**, *1*, 3−58.
[29] R. H. Blessing, *J. Appl. Crystallogr.* **1989**, *22*, 396−397.
[30] G. M. Sheldrick, *SHELXS-86: Program for the Solution of Crystal Structures*, Universität Göttingen, **1986**.
[31] N. K. Hansen, P. Coppens, *Acta Crystallogr.* **1978**, *A34*, 909−921.
[32] E. Clementi, C. Roetti, *Atomic Data and Nuclear Data Tables*, Academic Press, New York, USA, **1974**, *14*, 177−178.
[33] R. F. Stewart, E. R. Davidson, W. T. Simpson, *J. Chem. Phys.* **1965**, *43*, 175−187.
[34] D. T. Cromer, *International Tables for X-ray Crystallography* (Eds.: J. A. Ibers, W. E. Hamilton), Kynoch Press, Birmingham, England, **1974**, p. 148−151.
[35] F. H. Allen, *Acta Crystallogr.* **1986**, *B42*, 512−522.
[36] F. R. Thornley, R. J. Nelmes, *Acta Crystallogr.* **1974**, *A30*, 748−757.
[37] E. Clementi, D. L. Raimondi, *J. Chem. Phys.* **1963**, *38*, 2686−2689.
[38] P. Coppens, T. N. Guru, P. Leung, E. D. Stevens, P. Becker, Y. W. Yang, *Acta Crystallogr.* **1979**, *A35*, 63−72.
[39] M. Souhassou, E. Espinosa, C. Lecomte, R. H. Blessing, *Acta Crystallogr.* **1995**, *B51*, 661−668.
[40] F. L. Hirshfeld, *Acta Crystallogr.* **1976**, *A32*, 239.
[41] D. W. J. Cruickshank, *Acta Crystallogr.* **1949**, *2*, 65−82.
[42] B. Rees, *Acta Crystallogr.* **1976**, *A32*, 483−488.

Received November 24, 1998
[O98532]